GA–A23798

ELM ENERGY SCALING IN DIII–D

by
A.W. LEONARD, R.J. GROEBNER, M.A. MAHDAVI, T.H. OSBORNE,
M.E. FENSTERMACHER, C.J. LASNIER, and T.W. PETRIE

APRIL 2002

DISCLAIMER

GA–A23798

ELM ENERGY SCALING IN DIII–D

by
A.W. LEONARD, R.J. GROEBNER, M.A. MAHDAVI, T.H. OSBORNE,
M.E. FENSTERMACHER,† C.J. LASNIER,† and T.W. PETRIE

This is a preprint of a paper presented at the IAEA Technical Committee Meeting on Divertor Concepts, September 11–14, 2001 in Aix-en Provence, France and to be published in *Plasma Physics and Controlled Fusion.*

†Lawrence Livermore National Laboratory, Livermore, California

Work supported by
the U.S. Department of Energy under
Contracts DE-AC03-99ER54463 and W-7405-ENG-48

GA PROJECT 30033
APRIL 2002

1. INTRODUCTION

Edge-Localized Modes (ELMs) have been identified as a serious concern for the divertor of the next generation of tokamaks [1,2]. The periodic relaxation of the edge pressure gradient in H–mode results in a pulse of energy and prticles transported across the separatrix to the Scrape-Off-Layer (SOL) and eventually into the divertor. If the ELM deposits enough energy on the target the surface temperature can rise above the ablation threshold. Because of the many ELMs, perhaps thousands, that are expected in each discharge, exceeding the ablation threshold will result in excessive target erosion and an unacceptably short divertor lifetime. The surface temperature rise due to an ELM scales approximately with the deposited energy density and inversely with the square root of the heat pulse duration. For the divertor design for ITER-FEAT this threshold is expected to be 0.4 MJm^{-2} on a CFC divertor target and 0.64 MJm^{-2} for a tungsten divertor target material, assuming a deposition time of 0.3 ms. Previous studies in tokamaks [3–5] have found that 50%–100% of the energy released from the main plasma due to an ELM is deposited on the divertor target in an area of 1–2 times the steady-state heat flux between ELMs, with deposition times varying from 100 μs to 1 ms.

The energy released from the main plasma at each ELM remains a key parameter for divertor design of future large tokamaks. In general the ELM energy has been found to scale approximately with the magnitude of the H–mode pedestal pressure. This is not surprising since the ELM is essentially a relaxation of the steep edge gradients characteristic of H–mode operation. Further, a size comparison between DIII–D and JET found the ELM energy to be proportional to the edge pedestal pressure times the main plasma volume, or pedestal energy [1]. However this proportionality constant is not really a constant and has been found to vary significantly with density and/or pedestal collisionality [6,7]. Therefore, to predict the ELM size that will occur in future large tokamaks it is important to identify the processes that control the energy transport

during the ELM. This will hopefully lead to models than can be scaled to the larger size of future experiments.

This paper examines how energy is lost from the edge pedestal region due to an ELM with the goal of adding insight about the important energy transport processes. We present analysis which uses DIII–D Thomson scattering data to determine changes to the pedestal density and electron temperature profiles due to an ELM. The perturbed profiles are then integrated to determine the energy loss associated with convection, and the ELM energy due to conduction. ELM energy lost through these channels is then discussed in the context of parallel transport processes from the pedestal to the SOL and eventually the divertor target.

2. EXPERIMENTAL RESULTS

The series of discharges in this study were in a low triangularity, $\delta \approx 0$, lower single-null, LSN, configuration as shown in Fig. 1(a). Several discharges were at higher upper triangularity, $\delta \approx 0.4$, Fig. 1(b), to assess triangularity dependence. The discharges had variations in plasma current of 0.8–2.0 MA with variations in toroidal field of 1.4–2.1 T for a variation in safety factor q_{95} of 2.5–6.0. Pumping in this divertor configuration allowed for a range in pedestal density of $2–13\times10^{19}$ m^{-3} corresponding to a normalized pedestal density range of 0.2-0.9 times the Greenwald density, $n_{GW}(10^{20}m^{-3})= I_p(MA)/[\pi a^2(m)]$.

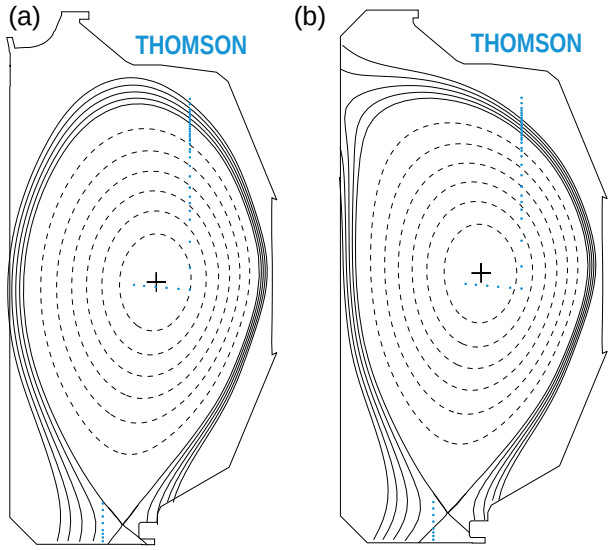

Fig. 1. Magnetic configuration used in this ELM study. Low triangularity configuration (a) with upper δ~0.0 and lower δ~0.0. High triangularity configuration (b) with upper δ~0.4 and lower δ~0.0. Divertor pumping provides density control in both cases. The Thomson measurement locations are also shown, as a vertical dotted line.

The primary tool for this study is the DIII–D Thomson scattering diagnostic. The viewing locations for this diagnostic are also shown in Fig. 1. The highest spatial resolution for the Thomson measurements is in the edge pedestal where steep gradients are found. Thomson scattering is a very fast measurement of T_e and n_e at a single point in time. The DIII–D system takes 80 such measurements each second. Over a period of 0.5–1.0 s of steady ELMing conditions the Thomson data can be ordered to the nearest ELM to give a temperature and

density profile across an ELM. A typical time window for this analysis is shown in Fig. 2. A divertor D_α signal is used to determine the ELM time. Shown also are the pedestal T_e and n_e with symbols at the measurement times of the Thomson scattering diagnostic.

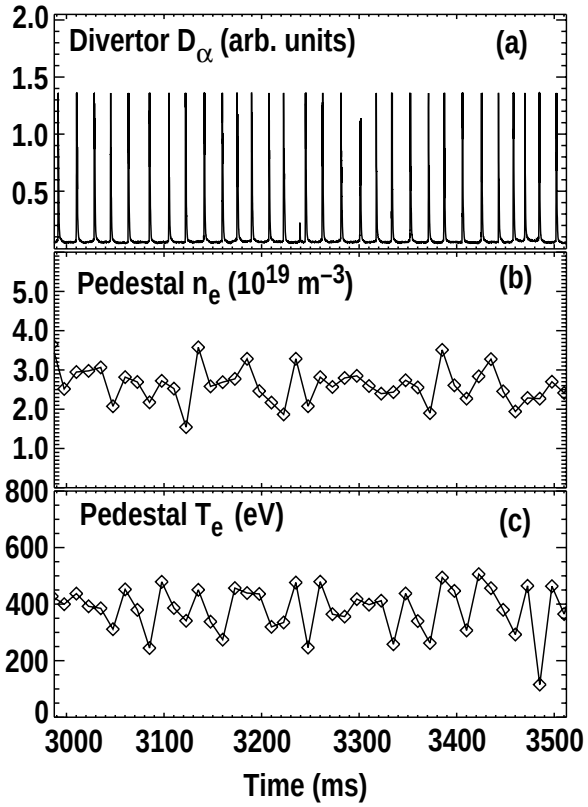

Fig. 2. A typical time window for the Thomson ELM profile analysis. (a) A divertor D_α signal is used to determine the ELM time. Shown also are the pedestal (b) T_e and (c) n_e with symbols at the measurement times of the Thomson scattering diagnostic.

The ordering with respect to the nearest ELM of the Thomson density and electron temperature data for a single channel near the top the edge pedestal is shown in Fig. 3. Clearly a trend can be seen in both T_e and n_e with values constant to slowly rising approaching an ELM, a sharp drop at the ELM and then rising again towards the next ELM. To arrive at a loss in T_e and n_e due to an ELM, the time dependence of the values are fit to a linear function prior to, and after, the ELM as also shown in Fig. 3. The difference in intercepts at t=0, the ELM time, determines ΔT_e and Δn_e at that measurement location. Though the time dependence might be expected to better fit an exponential function in accordance with the time evolution of stored

energy, for this preliminary study the fewer fitting parameters and simplicity of the linear fit was deemed more appropriate.

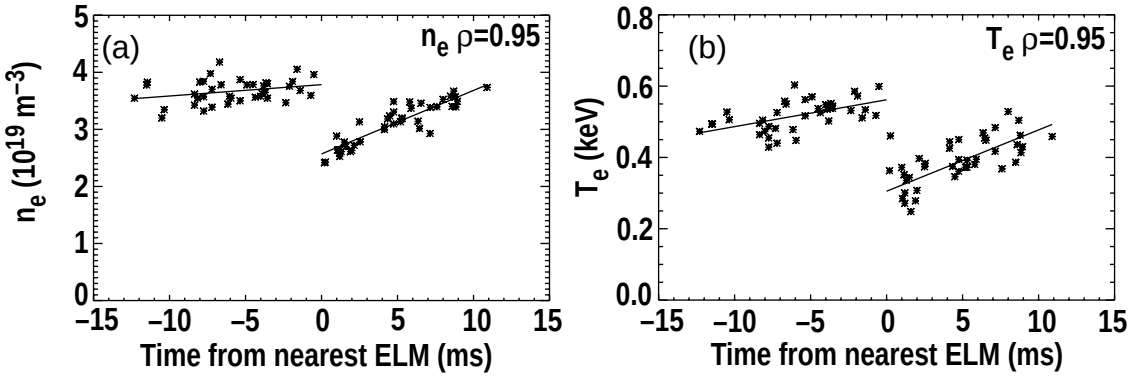

Fig. 3. Fitting of Thomson measurements at ρ=0.95 with respect to the nearest ELM. Both (a) density and (b) temperature are fit.

Finally the fits for all the measurement locations are combined into a profile for T_e and n_e just before, and just after an ELM, as show in Fig. 4. The measurement locations are converted to normalized radius, ρ, the square-root of toroidal flux, as determined through reconstruction of the magnetic equilibrium. The uncertainty in the location of the separatrix is ~5 mm, or Δρ~0.01. Clear changes can be seen in both the density and temperature profiles, peaking near the pedestal top, ρ≈0.96, and extending radially inward to ρ≈0.8. Inside of this location the perturbations quickly become negligible. Another instructive view of this data is shown in Fig. 5 where the relative changes to T_e and n_e are plotted. Here again the significant ELM perturbation extends from the separatrix into ρ≈0.8.

The profiles of Fig. 5 are somewhat surprising in that the perturbations are significantly wider than the steep gradient region that supposedly drives the ELM instability. Recent theoretical work [8,9] postulates that the ELM instability results from a coupled peeling-ballooning mode driven by both the edge pressure and current gradients. The predicted eigenmodes of this instability are much wider than the steep gradient region of the pedestal and qualitatively of a very similar shape to the profiles of Fig. 5. A direct comparison of the

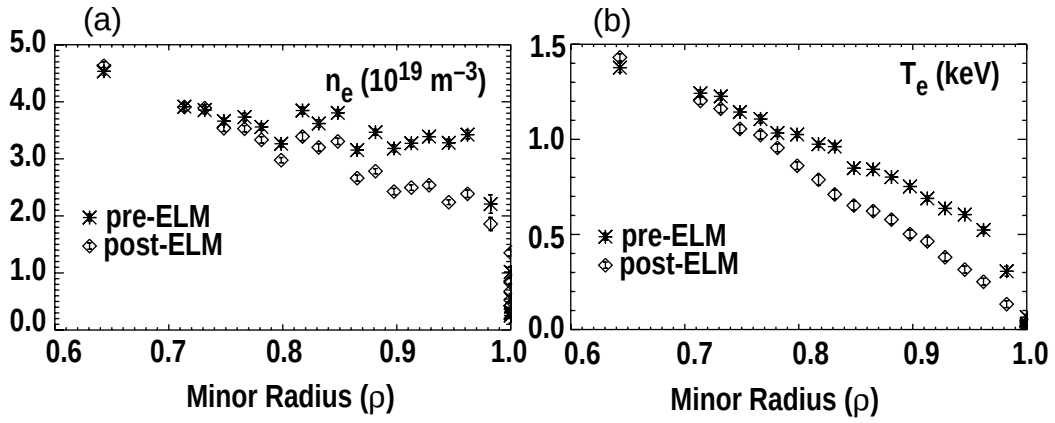

Fig. 4. Profiles of n_e and T_e as fit to before and after an ELM.

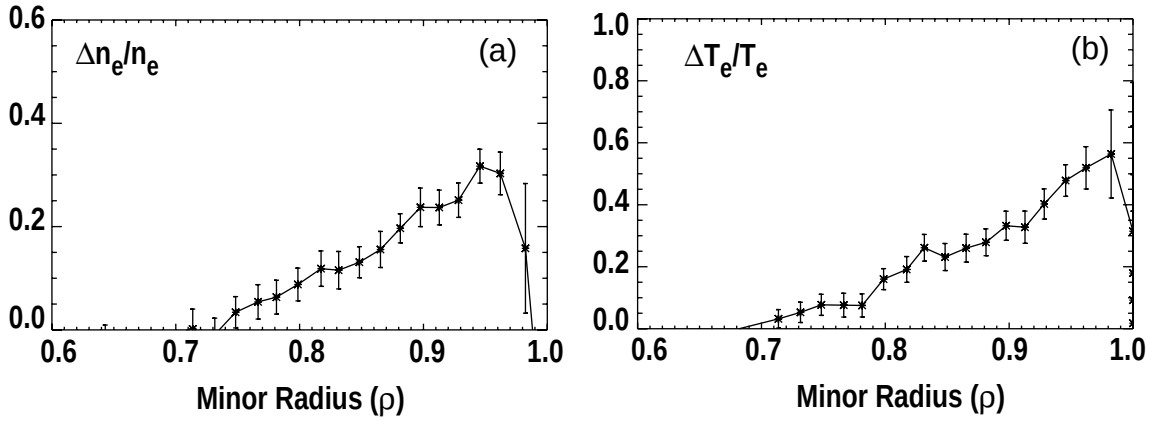

Fig. 5. Relative changes to the n_e and T_e profiles due to an ELM. The relative perturbation is defined and the difference between the pre- and post-ELM profiles divided by the pre-ELM profile.

perturbation profiles to this stability theory will be the focus of future work to better understand the ELM instability.

The primary concern of this study is the transport of energy from the plasma due to an ELM. The lost energy can be calculated for the electrons by integrating the profiles before and after an ELM. The energy can be split into two parts, convected and conducted energy. The convected energy, $T_e\Delta n_e$, is seen as changes to the density profile and represents plasma that is convected out of the main plasma into the SOL and divertor. Changes to the temperature profile represent conduction, $n_e\Delta T_e$, a loss of heat from the plasma inside the separatrix. For the ion energy lost at each ELM charge neutrality and $Z_{eff} = 1$ are assumed, resulting in equal electron and ion

convected ELM energy. A more accurate analysis using measured Z_{eff} profiles can be used in future analysis. The ion temperature profile, however, is assumed to not change across an ELM resulting in no ion conducted ELM energy. This assumption is motivated by the ion parallel thermal conductivity being smaller than the electron conductivity by $(m_e/m_i)^{1/2}$. Because ion temperature profiles with fast time resolution were not obtained for this data set, this assumption will have to be tested in future experiments. With the above assumptions the example profiles in Fig. 4 can be integrated over the plasma volume to arrive at a convected ELM energy of 12.5 kJ, split equally among electron and ions, and a conducted energy of 12.4 kJ, electron energy only, for a total of 25 kJ of lost plasma energy due to each ELM.

For part of the data set the ELM energy calculated from the Thomson profiles is compared in Fig. 6 to ELM energy calculated from fast magnetic equilibrium reconstruction of the plasma stored energy. The fast magnetic analysis represents an ELM energy averaged over the same time window as the Thomson profile data. The reasonable correlation of these two methods shown in Fig. 6 suggests credibility of the Thomson profile analysis. The rather large error bars for both methods arise from ELM to ELM variability as well as the inherent uncertainty in both measurements. For the fast magnetics analysis noise in the magnetic signals results in a measurement uncertainty of ~10 kJ. The remainder of the error is mostly ELM variability. The data of Fig. 6 would then suggest a ELM energy variability of ~20%. A similar size error in the Thomson analysis also suggests that this is a dominant factor in the uncertainty. The ELM variability is particularly large at high density where the ELMs become small and irregular. For these reasons ELM energies less than ~10 kJ are less than the measurement resolution. ELM variability will be important in assessing the potential for divertor ablation, however for this study we have only attempted to characterize an average ELM.

At the highest ELM energies the Thomson technique produces lower values than the fast MHD analysis. These occur at low densities where perturbations to T_e will be seen to be the greatest. A preliminary look at ion temperature measurements by CER for one of these cases indicate some perturbations to the ion temperature profile occur at each ELM. Future CER

measurements with improved time resolution will be required to determine the level of perturbation to the ion temperature profile.

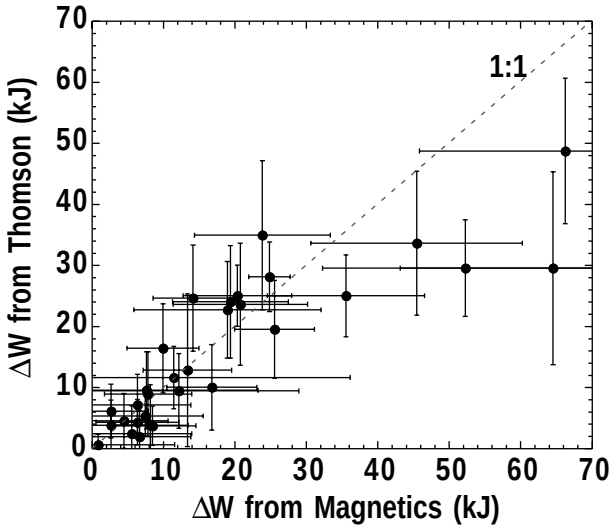

Fig. 6. ELM energy as measured by changes to the Thomson n_e and T_e profiles versus ELM energy as determined by fast magnetic equilibrium analysis.

The fitted Thomson pre- and post-ELM profiles were integrated separately for convected and conducted energy over the entire data set. The ELM energy lost due to convection is normalized to the pedestal energy and is plotted versus the pedestal Greenwald parameter, $n_{e,ped}/n_{GW}$ in Fig. 7(a). The conducted ELM energy over the same data set is plotted in Fig. 7(b). The pedestal energy is calculated as twice the pedestal electron pressure times the plasma volume, or $2\times3/2\times P_{e,ped}\times Vol$. This normalization of the ELM energy has been used successfully in the past for comparison between different tokamaks [1]. Density scans for four different cases are presented; high q, q_{95},~3.9, at 1.2 MA and 2.1 T; intermediate q, q_{95}, ~3.1, at 1.2 MA and 1.5 T; low q, q_{95}, ~2.5, at 2.0 MA and 2.1 T; and high triangularity, upper δ~0.4, at 1.2 MA and 2.1 T. It is important to realize that the pedestal pressure varies significantly over the data set. In general the pedestal pressure decreases significantly at high density, or collisionality, resulting in the ELM energy at high density decreasing much more than might otherwise be indicated in the figure.

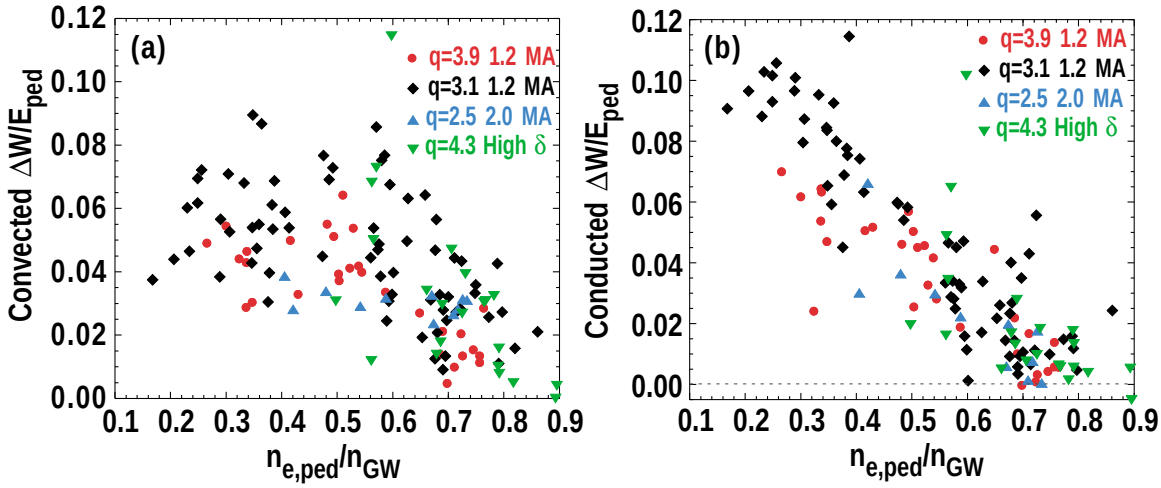

Fig. 7. (a) The normalized convected ELM energy as measured by the Thomson profile versus the pedestal density normalized by the Greenwald parameter, $n_{e,ped}/n_{GW}$. (b) The normalized conducted ELM energy versus the normalized pedestal density.

Several interesting trends can be seen in the data of Fig. 7. First, for the convected energy there is significant scatter in the data, but no obvious trend from low density until about $n_{e,ped}/n_{GW}$~0.65. There is also no obvious *q* dependence among the different cases. It should also be noted that the high current and high triangularity cases have approximately a factor two higher pedestal pressure, but the ELM energy remains approximately a constant fraction of the pedestal energy. At higher density, $n_{e,ped}/n_{GW}$>0.65, the normalized ELM convected energy drops significantly, to almost the measurement uncertainty. This is the same region where the pedestal pressure begins to degrade. The large relative scatter in the data in the high density region is mostly due to ELM variability where the ELMs are small and irregular, as earlier noted. The scatter is also amplified by ELM energy normalization to the pedestal pressure which is reduced at high density. However, there is no obvious reason for the relatively large scatter at low density for the convected energy measurements at q = 3.1. Though ELM variability may be responsible for this scatter it should be noted that the scatter is much smaller in the conducted energy analysis of the same data.

The conducted ELM energy shows a clear trend with density, with a maximum at the lowest density and decreasing to near zero at $n_{e,ped}/n_{GW}$~0.7. All four cases follow the same curve

within the measurement uncertainty. This implies a similar behavior for the conducted energy regardless of q, plasma current, triangularity, or the pedestal pressure. Density, or some related parameter, does seem to be playing a key role.

Instead of pedestal density, the pedestal electron collisionality, as a dimensionless parameter, might be more appropriate for ELM scaling. For example, the edge bootstrap current might be reduced at higher collisionality resulting in a change in the stability of the edge [10,11]. To check the ELM scaling with respect to collisionality the same ELM conducted and convected energy data is plotted in Fig. 8 versus the electron collisionality evaluated at the top of the pedestal. This scaling does not appear to fit as well as the normailized pedestal density. In particular the high plasma current and high triangularity data have a higher pedestal pressure, leading to a lower collisionality, at the same normalized density. The possible implications of different scalings will be examined later in this paper.

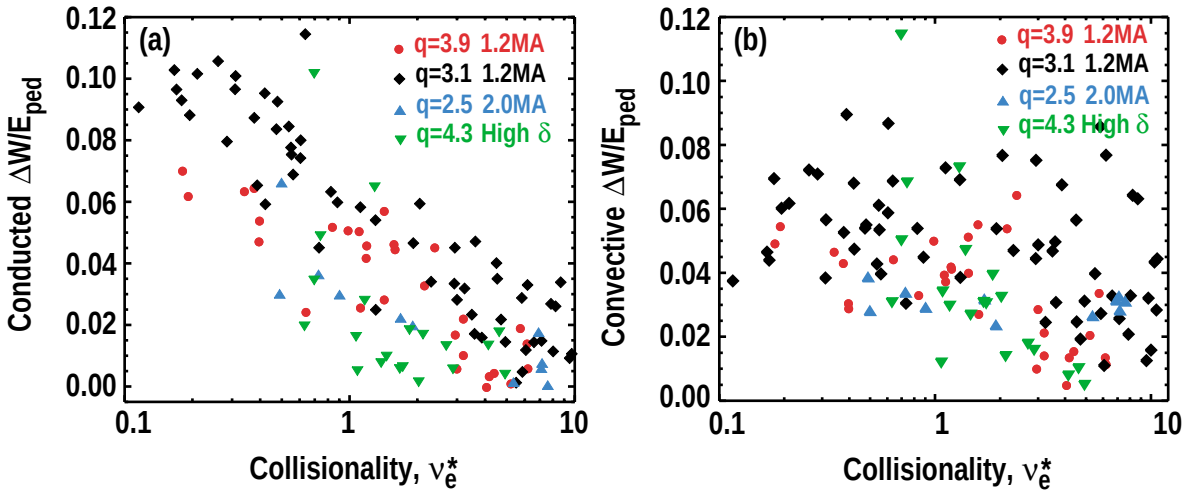

Fig. 8. The normalized (a) conducted ELM energy and (b) convected ELM energy versus the pedestal electron collisionality.

3. DISCUSSION: PARALLEL VERSUS PERPENDICULAR TRANSPORT LIMITS

A predictive capability for Type I ELM energy is the ultimate goal for this line of research. As a first step it is important to identify the processes that control the ELM energy transport. As a start two simple ideas can be discussed in light of this and previously observed data. The first conjecture is that the ELM instability results from an overlap of many MHD modes producing a stochastic layer in the pedestal region. Parallel transport, convection and/or conduction, then carries energy from the pedestal to the SOL and eventually the divertor. The pedestal energy drains away until the ELM instability ends and the door between the pedestal and the SOL is closed. In this model loss of density from the pedestal, or convective transport, would be limited to the ion sound speed for plasma leaving the pedestal and flowing into the SOL and eventually the divertor. Loss of pedestal temperature would be controlled by electron conduction, perhaps collisionless, to the divertor. The sheath at the divertor targets may also place a limit on the level of heat conduction to the divertor target. An alternative model for the ELM energy loss is the ELM instability, through fluctuation driven transport, equalizes the gradients across the separatrix where parallel transport then carries the energy to the divertor. The ELM energy would then be set by the level of perpendicular transport. Fast measurements of the density perturbation profile in the SOL would aid in assessing this possiblity.

The time scale for convective parallel transport should be the parallel connection length divided by the ion sound speed. The parallel field line length to the divertor from 0.5 cm outside the separatrix at the midplane is approximately 20 m in DIII–D. The field line length from the pedestal to the SOL will depend on details of the ELM instability and could vary considerably with different parameters. The ion sound speed for the discharges in this study varies from, ~2–4×10^3 m/s, for the pedestal temperature range of 200–700 eV in this data. This is a parallel time of 80–150 μs from the midplane to the divertor. The period of strong magnetic perturbations

during an ELM, as measured by magnetic probes, is similar at 200 μs. This could allow a significant fraction of the pedestal density to flow to the SOL and eventually the divertor. However, the fractional loss of density should get larger at low density and high pedestal temperature. This dependence is not seen, though a large scatter in the data could be hiding such behavior. Also, it is unknown what effective path length from the pedestal to the SOL would be created by the stochastic field lines of the ELM instability. Evaluating this path length will require accurate modeling of the ELM instability. Whatever path length results, however, the parallel electron heat conduction should be much larger than parallel convection. This will be discussed in the next section on conductive transport.

An alternative explanation for the perturbed density profile of Fig. 5 assumes a flat profile density profile from the pedestal top inward. The plasma lost at an ELM can be accounted for by equalizing the density from the pedestal out into the SOL with a width of 2–3 cm at the midplane. In fact, heat flux widths that have been measured on the divertor target of DIII–D are the order of this same 2–3 cm SOL width at the midplane [4].

A conjecture for the convective transport may then be the ELM instability, through turbulence or magnetic reconnections, relaxes the density gradient over some radial width from inside the pedestal across the separatrix out into the SOL. The density loss for the ELM instability does not appear to change character until the highest densities. This can be seen in the perturbed density profiles for low, moderate and high density shown in Fig. 9. The widths and amplitudes of the perturbed density profiles are also constant from low to moderate densities. At the highest densities the perturbed width becomes somewhat narrower and presumably the lost density is spread less deeply into the SOL. A smaller ELM due to a decreased width of the instability is supported by previous measurements of reduced magnetic fluctuation levels and increased mode number at high density [6,12].

The loss of electron temperature in the pedestal, or conductive transport, should occur on a much faster time scale than convective transport. Normal collisional parallel energy transport should take place at the electron thermal speed. Though the pedestal is relatively collisionless,

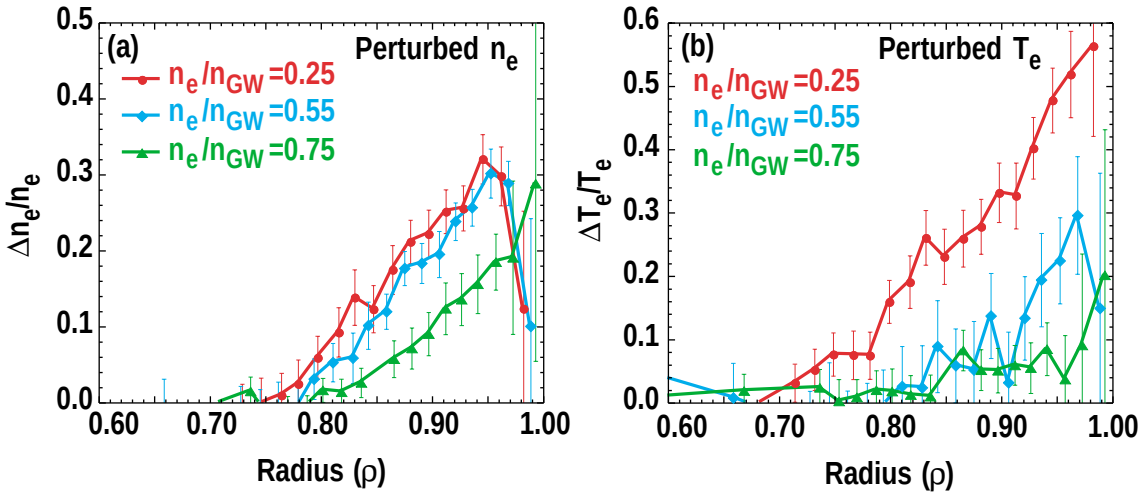

Fig. 9. (a) The perturbed density profile for three pedestal densities, $n_{e,ped}/n_{GW}$=0.25,0.55 and 0.75. (b) The perturbed T_e profile for the same three pedestal densities.

significant transport should still occur within the 200 μs duration of the ELM instability. Hot electrons can stream from the pedestal towards the divertor until a rising potential due to the slower ions confines them. However, colder electrons from the divertor can also move upstream to replace the hotter electrons resulting in collisionless conduction. The slowest time scale should be that of the thermal speed of the colder divertor electrons. For a divertor electron temperature of 10 eV the transport time should be ~ 20 μs, much shorter than the ELM duration or convective time. Even at 1 eV the transport time is only 60 μs. Parallel conduction does not appear to be a limiting factor for ELM energy transport.

Another factor that may limit parallel heat transport is the divertor target sheath potential [13]. As hot electrons stream into the divertor target raising the electron temperature the sheath potential rises to maintain charge neutrality. The target heat flux would then be limited by the number of ions crossing the sheath, essentially the ion saturation current. Further experimental work is required to determine if this process is limiting ELM energy in DIII–D. A fast measurement of T_e in the divertor, the ion saturation current, and the target heat flux would be useful to resolve this issue.

A common observation of ELM divertor target heat flux might be explained by sheath considerations. On a number of tokamaks the ELM heat flux is usually greater at the inboard

target compared to the outboard by a factor of 2–3 [1]. This is perplexing in that the radial ELM transport is thought to originate at the outer midplane in the region of bad curvature, transporting the heat flux closer to the outboard divertor. If, however, fast parallel transport raises both the inboard and outboard electron temperature to the same level, then the in/out ratio of ELM heat fluxes will be set by the in/out ratio of saturation current. This effect would imply a pressure imbalance that might occur on a short time scale before the divertor ions could respond to the ELM flux. Interestingly, it is also often observed that the density and ion flux is greater to the inboard target in single-null discharges between ELMs.

It is not clear how to associate the conductive transport trend of Fig. 7 with parallel transport issues. Greater conductive losses are seen at high pedestal temperature and/or low collisionality. This can also be seen in the perturbed T_e profiles of Fig. 9(b). At lower density and higher T_e parallel conductivity will be higher, but it is already much greater than needed for the observed ELM heat flux. It is possible that the divertor target sheath may be limiting the heat flux, but the experimental dependence is opposite to what might be expected. The divertor density, and thus the ions available to cross the sheath, has been observed to increase faster than the line-averaged density or pedestal density. This would imply the heat should increase with pedestal density. More experimental data from the divertor, particularly fast measurements of T_e are needed to investigate this process.

Another possibility for conductive transport is that it is limited by the character of the ELM instability itself in transporting heat from the pedestal to the SOL where it can be conducted rapidly to the divertor by parallel processes. Parallel conduction would be fast enough to drain significant energy from the pedestal and SOL on the timescale of the ELM instability. This might also account for perturbations to the ion temperature as well. Even though the parallel ion conductivity is much less than that of the electrons, fluctuation driven perpendicular ion conduction and parallel ion conduction in the SOL may still be sufficient for significant energy transport.

The difference in parallel transport times for conduction compared to convection could account for the different density dependencies of ELM convected and conducted energies. From moderate to low density the ELM fluctuations more rapidly mix the pedestal temperature profile with the SOL. The higher temperature is quickly drained to the divertor. For the density profile, however, the convective losses in the SOL are slower. The parallel flow in the SOL would then be the limiting process and might show less of a density dependence than the conductive losses. At high density, $n_{e,ped}/n_{GW} \sim 0.7$, the ELM changes further with perpendicular transport occurring over a narrower region of the pedestal and SOL resulting in a narrower density perturbation and smaller convected energy. In addition, at high density the temperature perturbation and conducted energy become negligible.

4. CONCLUSIONS

In this study we have identified several characteristics of ELM energy loss that we have used to conjecture about the physical processes that may be most important for ELM energy transport. We can also conjecture about how these results may be used to scale ELM energy to future tokamaks such as ITER-FEAT. If ELM energy were to be governed by parallel plasma transport due to stochastic field lines created in the pedestal, then in a larger device the longer parallel lengths would result in a smaller convected fraction of the pedestal energy. The conducted ELM energy though would be quite large at the expected higher electron temperatures. Though the divertor sheath does not appear to limit the ELM conducted heat flux in DIII–D, the sheath may present a limit in larger tokamaks. This would depend on the scaling of the sheath parameters compared to the pedestal energy in a larger device. The DIII–D data presented here would indicate that the perpendicular transport, driven by turbulence or magnetic reconnection during an ELM could be the more important process. If only parallel transport processes are involved, electron conduction should be much larger than the observed convected energy. The data also indicates that the fraction of pedestal energy lost at an ELM becomes small as the pedestal density is increased above 0.65 n_{GW} across a variety of configurations and collisionalities. This is a somewhat hopeful result in that ITER-FEAT is expected to operate at a high normalized density. However, this study should not rule out the possibility that the normalized ELM energy actually scales with the pedestal collisionality. This would result in very large ELMs for the ITER-FEAT expected pedestal parameters and could seriously affect the ITER-FEAT divertor lifetime. Further work is needed as more appropriate scalings might be found with careful study. It is possible, for example, that the important collisionality is at the foot of the pedestal which could show the same trend as plotted for DIII–D, but might scale differently to larger tokamaks.

While further work is certainly needed for the study of Type I ELMs, other options should also be explored. At high triangularity and/or density, smaller irregular perturbations to the

pedestal, or Type II ELMs, have been found. It is important to expand studies of these acceptable ELMs to determine if their operational space can be exploited by the next generation of larger tokamaks.

REFERENCES

[1] A.W. Leonard, et al., J. Nucl. Mater. **266-299** 109 (1999).

[2] G. Janeschitz, et al., J. Nucl. Mater. **290-293** 1 (2001).

[3] A. Herrmann, et al., Plasma Phys. Control. Fusion **37** 17 (1995).

[4] A.W. Leonard, et al., J. Nucl. Mater. **241-243** 628 (1997).

[5] R. Mohanti, et al., Proc. 24th European Conf. on Controlled Fusion and Plasma Physics, June 1997, Berchtesgaden, Germany, **Vol. 21A, Part 1, 101** (European Physical Society, 1997).

[6] A.W. Leonard, et al., J. Nucl. Mater. **290-293** 1097 (2001).

[7] A. Loarte, et al., Proc. 18th IAEA Fusion Energy Conference, Sorrento, Italy (2000).

[8] J.W. Conner, et al., Phys. Plasmas **5** (1998) 2687.

[9] P.B. Snyder, H.R. Wilson, J.R. Ferron, et al., "Edge Localized Modes and the Pedestal: A Model Based on Coupled Peeling-Ballooning Modes," accepted for publication in Phys. Plasmas (2002).

[10] O. Sauter, et al., Phys. Plasmas **6** 2834 (1999).

[11] T.H. Osborne, et al., J. Nucl. Mater. **266-299** 131 (1999).

[12] T.H. Osborne, et al., Phys. Plasmas **8**, 2017 (2001).

[13] Shimada, et al., ITER Design Report, Plant Description, Chapter 4.5.2, to be published by IAEA.

ACKNOWLEDGMENT

Work supported by U.S. Department of Energy under Contracts DE-AC03-99ER54463 and W-7405-ENG-48.